# Intensity fluctuations of radiation scattered in the near-ground atmospheric layer from a focused laser beam. Part 1. Snowfall

**N.A. Vostretsov and A.F. Zhukov**

*Institute of Atmospheric Optics,*
*Siberian Branch of the Russian Academy of Sciences, Tomsk*

Received June 22, 1999

Fluctuation characteristics of a focused laser radiation scattered in snowfall are analyzed in the single-scattering approximation. Some salient features of the fluctuations have been revealed.

From the general physical principles it is clear that fluctuations of scattered radiation depend on many parameters. Among the most important factors influencing the fluctuation of scattered radiation are optical properties of scatterers, their velocities, atmospheric turbulence, size of a photodetector, distance from the optical axis of the beam $\Delta L$, optical depth $\tau$, separation between the source and a receiver $L$, and others. The role of each parameter is not yet completely determined, but individual influence can be qualitatively predicted.

In this paper we analyze experimental results on some temporal characteristics of the speckle structure of laser radiation in the focal plane near the optical axis of a focused laser beam in snowfall under single-scattering conditions. Statistical characteristics of the intensity of scattered radiation are measured at a fixed distance from the optical axis in order to find such peculiarities in fluctuations of the scattered radiation that are indicative of weather conditions in the near-ground atmospheric layer.

This paper is a continuation of our investigations reported in Ref. 1.

## 1. Experimental setup

In the discussed experiment the values of $\Delta L$, $L$, the beam diffraction parameter $\Omega$, and the curvature radius of the phase front of the beam $R$ ($R = -L$) were kept constant. Under such conditions we studied the influence of the optical depth $\tau$, wind velocity $V$ and $V_\perp$, and the maximum size of snow flakes $D_{max}$ on the fluctuation characteristics of scattered radiation.

Figure 1 shows optical arrangement of measurements. The laser beam from an LG–38 He–Ne laser was expanded with the lenses L1 and L2 so that its Fresnel parameter $\Omega$ in the plane of the source was equal to 50. Here $\Omega = k\,\alpha_2^0/L$, where $k = 2\pi/\lambda$; $\alpha_0$ is the effective radius of the beam; $L$ is the distance which the beam passes in the atmosphere ($L = 130$ m). Specifications of the laser source: $\lambda = 0.63$ μm, output power $P \le 70$ mW, divergence angle $5 \cdot 10^{-4}$ rad; the radiation was linearly polarized with the polarization plane normal to the Earth's surface. The beam was focused at a distance $L = 130$ m, and the beam diameter of the focused spot was estimated visually to be no more than 5 mm. To focus the beam, the lens L1 was moved along the optical axis of the lens L2. The lenses L1 and L2 together made up a high-quality collimator of an OSK–2 optical bench. The lens L2 has 16-cm diameter and the focal length of 160 cm. The receiving diaphragm installed in front of the photodetector had the diameter of 0.01 cm. A cylindrical 110-cm-long blend was set in front of the diaphragm; three round diaphragms of 3-cm diameter were installed inside the blend centered about its axis. The photodetector field of view was $2.7 \cdot 10^{-2}$ rad. The optical depth $\tau$ of the 130-m-long path was calculated from the data of the RDV–3 transmissometer operated on the path of 100×2 m length. It was operated at the receiving end of the path near the laser beam. The maximum size of snow flakes, $D_{max}$, was estimated by eye upon their sedimentation on a fur surface. The wind speed $V$ and its direction were measured with an M63m device at the altitude of 2.5 m; these data were used for calculation of the wind velocity component $V_\perp$, which was normal to the path. The path was 2.5 m above the ground.

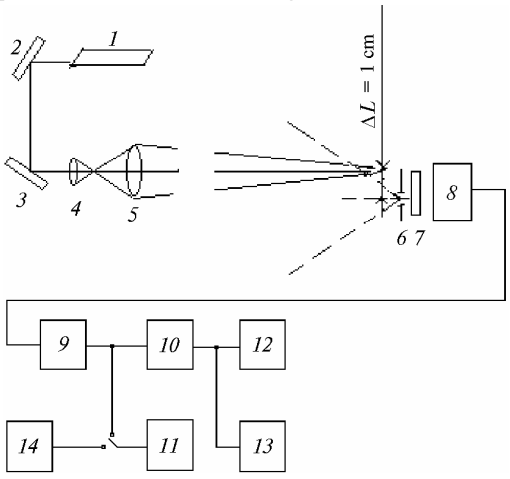


**Fig. 1.** Optical arrangement of measurements: laser (*1*); plane mirrors (*2* and *3*); lenses L1 and L2 (*4* and *5*); diaphragm (*6*); interference filter (*7*); FEU–38 photodetector (*8*); amplifier (*9*); U5–10 amplifier (*10*); FSP–38 spectrum analyzer (*11*); AI–1024 pulse analyzer (*12*); X6–4 correlator (*13*); NRJ–20 noise generator (*14*).

0235-6880/99/08 660-05 $02.00 

We used the following measurement technique. First, the photoreceiving unit together with the blend was set on the optical axis of a focused beam. The criterion of the correct positioning was the maximum value of the mean signal at the output of the photomultiplier tube (PMT). In this case a strong neutral density filter (attenuator) was set in front of the PMT; then the receiving unit and the blend were shifted as a whole by 1 cm off the optical axis of the focused beam with the use of special micro-screws, and then the neutral density filter was removed. The frequency spectrum, autocorrelation function, and probability histogram of fluctuations were measured at the same time. According to our estimates, these characteristics were measured accurate to 15%. For every realization we determined $\tau$, $D_{max}$, $V$, and $V_\perp$, as well as the type of atmospheric turbidity determined by an operator who observed the weather.

## 2. Measurement results

### Normalized autocorrelation function (NAF)

In the experiment we obtained 130 records of NAF at different values of $\tau$, $D_{max}$, $V$, and $V_\perp$ with a specialized X6–4 device for studying the correlation characteristics. Our analysis included a total of 13 measurement series obtained in the winter period of 1998/99.

**Table 1**

| $D_{max}$, mm | $V_\perp$, m/s | $t_{cor}$, μs | | | | $N$ |
|---|---|---|---|---|---|---|
| | | 0.5 | 0.36 | 0.1 | 0 | |
| 1 | 4 – 4.4 | 116 | 163 | 284 | 340 | 4 |
| 1 | 1 – 2 | 311 | 416 | 746 | 1175 | 5 |
| 1 | < 1 | 360 | 489 | 1280 | – | 5 |
| 3 | 2.1 – 2.9 | 380 | 446 | 764 | 1010 | 4 |
| 3 | 1 – 2 | 442 | 606 | 1120 | 1891 | 15 |
| 3 | < 1 | 822 | 1059 | 1750 | 3265 | 3 |
| 7 | 7.2 | 92 | 108 | 167 | 205 | 1 |
| 7 | 3.6 | 211 | 286 | 414 | 474 | 1 |
| 7 | 0.6 – 0.9 | 516 | 613 | 1394 | – | 3 |
| 7 | < 0.2 | 907 | 1173 | 1575 | 1697 | 3 |
| 10–20 | 3 | 386 | 520 | 1600 | – | 1 |
| 10–20 | 0.6 | 517 | 720 | 1457 | 4750 | 3 |
| 10–20 | 0.1 | 912 | 1153 | 1775 | – | 3 |
| Haze, | 4.9 | 336 | 443 | 650 | 1200 | 1 |
| traces of | 4.3 | 538 | 680 | 1020 | 1157 | 1 |
| precipita- | 2.2 | 600 | 786 | 1075 | 1200 | 1 |
| tion | 0.3 | 925 | 1250 | 1634 | 1900 | 1 |
| | 0.0 | 1280 | 1680 | 2100 | 2330 | 1 |

For every NAF we calculated the correlation time $t_{cor}$ at which this function fell off down to the values of 0.5, 0.36, 0.1, and first reached zero value, i.e., $t_{cor}$ = 0.5, 0.36, 0.1, and 0. The correlation times $t_{cor}$ were analyzed in the following order. First, for all NAF's we studied the dependence of $t_{cor}$ on $V$ and $V_\perp$. It was found that no explicit dependence of $t_{cor}$ on $V$ and $V_\perp$ exists at different values of $D_{max}$. Then, the values of $t_{cor}$ were sorted by $D_{max}$ and $V_\perp$. The results are shown in the Table 1. One can see from the table that in snowfall $t_{cor}$ at the level of 0.5, 0.36, and 0.1 decreases with increasing transverse component of the wind velocity ($V_\perp$), at all values of $D_{max}$. The same tendency is characteristic of the haze at a very weak precipitation (traces of precipitation). The column $N$ of the table gives the number of NAF's used to obtain $t_{cor}$. However, as follows from the table, the correlation time may take close values (for example, $t_{cor}$ = 310–390 μs) at significantly different $D_{max}$ and $V_\perp$. It seems likely that $t_{cor}$ = 0.1 and other $t_{cor}$ depend on the ratio of the speed of particle motion to the characteristic size of particles. In a polydisperse medium, as a characteristic size we can take the mean size of particles and their speed.

Figure 2 demonstrates the change of NAF ($B(t)$) at close $D_{max}$ but different $V_\perp$ (Fig. 2*a*), as well as at close $V_\perp$ but different $D_{max}$ (Fig. 2*b*).

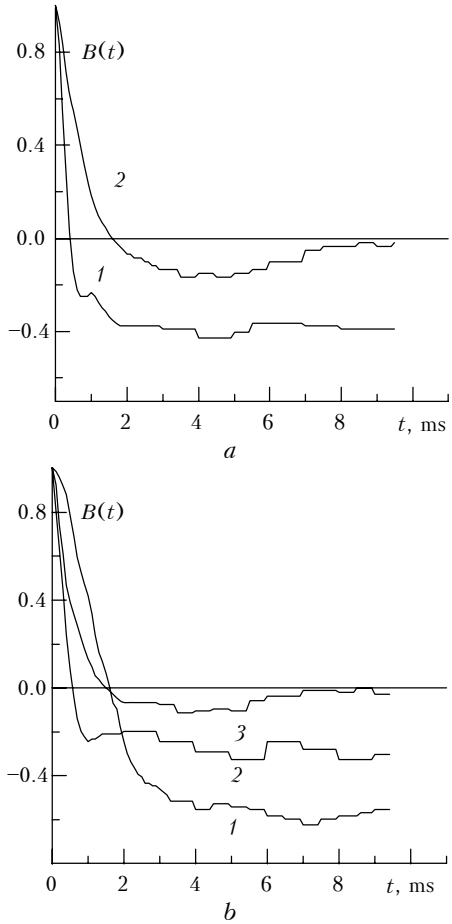


**Fig. 2.** Normalized autocorrelation functions: (*a*) $D_{max}$ = 3–5 mm, $V_\perp$ = 4.9 m/s, $\sigma^2_{exp}$ = 0.29, $\tau$ = 0.21 (curve *1*), $D_{max}$ = 3–5 mm, $V_\perp$ = 1.3 m/s, $\sigma^2_{exp}$ = 0.74, $\tau$ = 0.32 (curve *2*); (*b*) $D_{max}$ = 10 mm, $V_\perp$ = 1.5 m/s, $\sigma^2_{exp}$ = 0.32, $\tau$ = 0.43 (curve *1*), $D_{max}$ = 1 mm, $V_\perp$ = 1.7 m/s, $\sigma^2_{exp}$ = 0.25, $\tau$ = 0.38 (curve *2*), $D_{max}$ = 3–5 mm, $V_\perp$ = 1.7 m/s, $\sigma^2_{exp}$ = 0.22, $\tau$ = 0.1 (curve *3*).

### Temporal frequency spectrum

The temporal frequency spectrum was measured with a FSP–38 parallel spectrum analyzer. The output (mean) signals from every filter and the average-value channel were sent to a printer through a commutator.

They were used to calculate the spectrum of fluctuations of the received signal. The spectrum was normalized to its own variance: $U(f) = f_i \times W(f_i) / \int W(f_i)\, df_i$, where $W(f_i)$ is the spectral density of signal at the frequency $f_i$. The FSP–38 analyzer was calibrated with the help of a NRJ–20 generator of the "pink" noise. This calibration accounted for changes in the filter amplification coefficient. The spectral density of the "pink" noise decays in the inverse proportion to the frequency, so the signals at the cathode-ray tube (CRT) of the device, after passage through the filter, are almost equal to each other. This allows a real-time visual control over the analyzer functioning from observing signals on the CRT screen. The results of calibration were taken into account in calculations of $U(f)$. In the coordinates $U(f) = F(\log f)$ the area between two frequencies corresponds to the contribution of the frequency region into the measured variance of fluctuations $\sigma^2_{\text{exp}}$. We used this fact, as in Ref. 1, to estimate the turbulent contribution $\sigma^2_t$ into the measured variance $\sigma^2_{\text{exp}}$, and $\int W(f)\, df = 1$. The latter fact was used to check the correctness of our computations.

Our analysis included 26 spectra. It was found that the shape of the spectrum varies with time thus complicating revealing typical peculiarities in it. Nevertheless, we have managed to find some peculiarities in the shape of spectra characteristic of snowfalls.

(a) In a snowfall the hydrometeor maximum in the spectrum depends on $D_{\max}$ at close values of $V$ ($V_\perp$). With increasing $D_{\max}$ this maximum shifts toward lower frequencies. As $D_{\max}$ increases from 1 to 10, the maximum in the spectrum shifts by about an order of magnitude toward low frequencies.

(b) Most often the spectrum is asymmetric about the frequency of the hydrometeor maximum $f_{\max}$, that is, $\Delta f_r > \Delta f_{\text{left}}$, where $\Delta f_r$ is the right halfwidth determined at the level of 0.7; $\Delta f_{\text{left}}$ is its left counterpart.

(c) The width of the spectrum $\Delta f = \Delta f_r + \Delta f_{\text{left}}$ in the data analyzed varies from 150 to 600 Hz.

(d) In the coordinates $\lg [U(f)] = F [\lg f]$ at $f < f_{\max}$ and in some cases at $f \le f_{\max}$ the spectrum has a characteristic linear slope, which is described by the dependence $U(f) = A f^{\alpha}$ ($A$ is the coefficient). From these data the slope ($\alpha$) varies from 1 to 1.4.

(e) In the region of lowest frequencies, at $f \le 10$ Hz, there is a pronounced peak in the spectrum, which is most likely, due to the turbulence. The spectrum at $f \le 10$ Hz was used to estimate the turbulent contribution $\sigma^2_t$ into the measured variance $\sigma^2_{\text{exp}}$. The ratio $\sigma^2_t / \sigma^2_{\text{exp}}$ varies from 0.05 to 0.26.

(f) At $f > f_{\max}$ the spectrum sharply decays . We used two pairs of different coordinates to describe the spectrum at $f > f_{\max}$. In the coordinates $\log [U(f)] = F$ ($f$, kHz) the spectrum at $f > f_{\max}$ decays linearly. In 20 cases of total 26 cases it is described by the dependence $U(f) = A' \cdot 10^{-\gamma f}$ accurate to 10–15%. In the coordinates $\log [U(f) / U_{\max}] = F(f - f_{\max} / \Delta f)$ most spectra at $f > f_{\max}$ also have a linear section near the maximum value of $U(f)$ at $f > f_{\max}$.

(g) We failed to find a somewhat clear dependence of $\Delta f$, $\alpha$, and $\gamma$ on $D_{\max}$ and $V$ ($V_\perp$); this fact likely follows from the small number of spectra analyzed. This restricts the possibilities of making multi-parameter analysis.

## Distribution of the probability density (DPD) of fluctuations

Here it should be emphasized that reliable choice of some or other probability distribution based on the available theoretical literature is rather complicated. For this purpose we have analyzed 98 distributions. In our case the initial information was the distribution histogram. Its shape was analyzed in real time using the oscilloscope of the AI–1024 pulse analyzer employed.

Let us describe the technique of DPD measurements with AI–1024 device in a more detail. This device has 1024 levels (we used only 128). The dynamic range of the signal under study was 0.2 to 10 V. "ecause the signal can take values less than 0.2 V, zero of the UA–10 pre-amplifier was shifted to the value a little bit above 0.2 V. This shift was measured by a digital voltmeter and then taken into account in the processing. According to its manual, the AI–1024 analyzer estimates the probability density accurate to 5%. One sample in the AI–1024 analyzer lasts 1 μs. The quantization frequency ($f_q$) was chosen with the allowance for the correlation time $t_{\text{cor}}$ so that $1/f_q \ge t_{\text{cor}}$. As $t_{\text{cor}}$ we took the correlation time at the level 0.1. It was measured by an u 6–4 correlator in real time, so the analyzed samples of the signal correlated only weakly.

From visual observations it follows that the distribution is unimodal and has asymmetry towards its right-hand part. These are the important characteristics of the distribution. Several distributions with such peculiarities are known.[2] One of our goals was to find such a function, which describes the empirical diagram (distribution). This is a traditional goal of such analysis. However, it turned out hard-to-achieve, because the widely used method of straightened diagrams has low efficiency for integral distributions. Even good correspondence of the gamma-distribution to the empirical distributions obtained by the method of straightened diagrams is not supported by the classical $\chi$-square[2] and the Kolmogorov – Smirnov[3] criteria.

In this connection we sought other distributions. Toward this end, we calculated estimates for the parameters $\beta_1$ and $\beta_2$ by the histogram[2] ($\beta_1$ is the square of the normalized index of asymmetry, and $\beta_2$ is the normalized index of peakedness). Then the method of Pearson diagrams[2] was used. The idea of this method is that a certain place can be assigned to same number of known families of distributions in the plane

$\beta_1$ and $\beta_2$. Figure 3 shows curves *1–5* and the regions I and II between them. This figure uses the same scale as in Ref. 2. Curve *1* in Fig. 3 corresponds to the lognormal distribution; curve *2* corresponds to the gamma-distribution; zone I is for the beta-distribution, and region II is for the J-shaped beta-distribution. The point with coordinates $\beta_1 = 0$ and $\beta_2 = 3$ corresponds to the normal (Gaussian) distribution, while the point $\beta_1 = 4$, $\beta_2 = 9$ corresponds to the exponential distribution. Calculated values of $\beta_2$ and the corresponding values of $\beta_1$ at different $D_{max}$ are also shown in Fig. 3. It is seen that the experimental values in the plane ($\beta_1$, $\beta_2$) mostly occupy the zone characteristic of the beta-distribution. The dependence on the particle size ($D_{max}$) is not observed. Moreover, some distributions give the values of $\beta_1$ and $\beta_2$, which lie near curve *2* corresponding to the gamma-distribution.

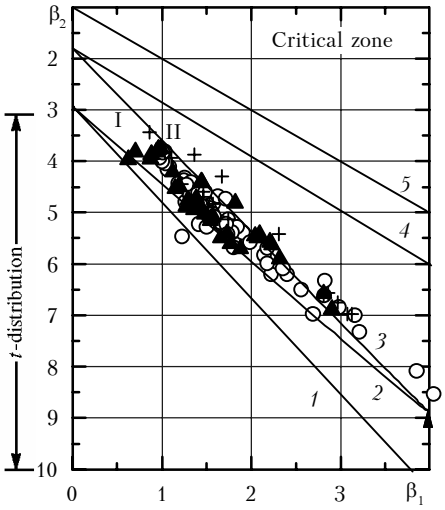


**Fig. 3.** Zones in the plane ($\beta_1$, $\beta_2$) for different distributions.

Remind that the beta-distribution is adequate for description of a random parameter whose values are limited to a finite interval.[2] "y this peculiarity, the beta-distribution is preferred for our measurements which were conducted at $U_{min} > 0.3$ and $U_{max} = (10 \pm 1)$ V.

A selective check of the generalized beta-distribution for the correspondence to the empirical distribution by $\chi$-square criterion and the Kolmogorov–Smirnov criterion[3] has shown that, according to these criteria, the empirical distributions are not described by the beta-distribution. Parameters of the generalized beta-distribution were estimated with the help of Ref. 2 and taking into account the values of $U_{min}$ and $U_{max}$ for every empirical distribution. As seen from Fig. 4, the best beta-distribution is in rather poor agreement with the empirical one in the presence of intensity spikes. The same is true for the gamma-distribution as well.

The estimates of $\beta_1$ and $\beta_2$ can be used to find the Johnson distribution[2] which is used for description of empirical distributions in some cases. From Fig. 5 it follows that for our purposes the Johnson $S_b$ distribution (three-parameter distribution) can be used. The parameters and criteria of agreement for this distribution will be calculated later on.

It should also be noted that we used the method of straightened diagrams for studying the lognormal and Rice–Nakagama distributions which are very far from agreement with the empirical distributions.

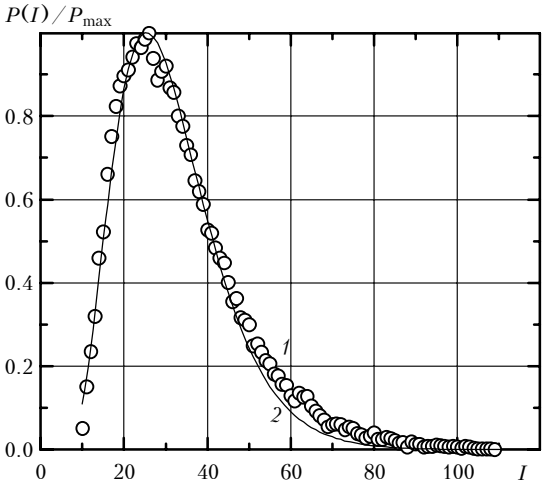


**Fig. 4.** Comparison of the empirical distribution (*1*) with the beta-distribution (*2*): $D_{max} = 1$ mm, $\sigma^2_{exp} = 0.29$, $\tau = 0.21$ (*1*); parameters of the beta-distribution: $\gamma = 2.24$, $\eta = 7.5$ (*2*); $I$ is the number of a channel; $P$ is the probability density; $P_{max}$ is the maximum value of the probability density.

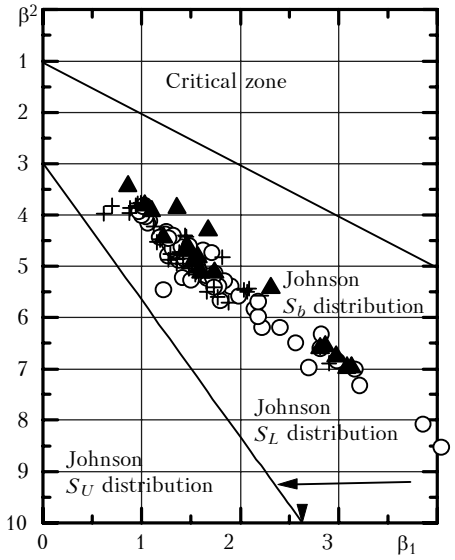


**Fig. 5.** Plots for selection of the corresponding approximating Johnson distribution: flakes $D_{max} > 5$ mm (+); $D_{max} = 1–5$ mm (○); $D_{max} \le 1$ mm (▲).

Further, distributions will be sought in the class of three-parameter distributions (with the use of $S_b$ and the generalized gamma-distribution).

### Variance of the intensity fluctuations

The normalized variance $\sigma^2_{exp}$ was calculated from the histogram (taking into account the bias). We failed to reveal a dependence of the variance on $\tau$ and $D_{max}$, which was reported in Ref. 1. The cause of this discrepancy between Ref. 1 and the data analyzed in this work is still unclear. At the same time, the values of $\sigma^2_{exp}$ calculated from the histogram of the probability density in this paper well agree with the variances measured by a variance meter.[1] The difference between them is only several percent.

## 3. Conclusion

Analysis of different statistical characteristics of the focused laser beam scattered in snowfall has enabled us to reveal some peculiarities characteristic of the intensity fluctuations. Most important peculiarity among them is a significant (by an order of magnitude) increase in the frequency of fluctuations in comparison with fluctuations on the optical axis of a focused beam, where they are mainly caused by the atmospheric turbulence. The role of turbulence in fluctuations of the scattered radiation decreases as compared with fluctuations in the direct beam intensity, but it is still pronounced in the shape of the spectrum of fluctuations and must be implicitly pronounced in other fluctuation characteristics. Thus, we can say that identification of weather conditions only by fluctuations of scattered radiation low efficient. Misinterpretation is possible, for example, when distinguishing between a dense haze and a weak precipitation. To exclude misinterpretation, additional measurements of the wind velocity and maximum size of particles are needed, so the capabilities of the purely optical method are significantly limited. Simultaneous measurements of fluctuations at two or more scattering angles in the direct beam probably opens up new capabilities. We plan to conduct such measurements in the future.

### Acknowledgments

We thank A.G. "orovoi for useful advice on the problems discussed in this paper.

The work was partially supported by the Russian Foundation for "asic Research, Project No. 99–02–16923.

### References

1. N.A. Vostretsov and A.F. Zhukov, Atmos. Oceanic Opt. **7**, No. 1, 12–15 (1994).
2. G. Hahn and S. Shapiro, *Statistical Models in Engineering Problems* [Russian translation] (Mir, Moscow, 1966), 395 pp.
3. L.N. Bol'shev and N.V. Smirnov, *Tables of Mathematical Statistics* (Nauka, Moscow, 1983).